Nuclear magnetic resonance pore-scale investigation of permafrost and gas hydrate sediments

R. L. KLEINBERG
Schlumberger-Doll Research, Ridgefield, CT 06877, USA

Abstract: Permafrost is a ubiquitous feature of arctic landmasses, and natural gas hydrate occurrence is widespread in the arctic and beneath the sea floor on continental slopes at all latitudes. The mechanical, thermal and hydraulic properties of the subsurface are profoundly modified by ice and hydrate. Nuclear magnetic resonance is a relatively recent addition to the measurement methods used to characterize recovered samples. This review shows how magnetic resonance has been used in two field studies to quantify frozen and unfrozen components of the sediment pore space, to understand the growth habit of ice and hydrate in rock and sediments, and to estimate hydraulic permeability.

It is well known that frozen soils cover a substantial fraction of the land surface of the Earth. It is less well known that vast areas of submarine continental slopes are also frozen due to the presence of gas hydrate, an ice-like solid with a melting point well above 0 °C at the elevated pressures found beneath the bottom of the ocean (Kvenvolden 1993). Permafrost- and gas-hydrate-affected sediments have considerable practical importance. Cold region and deep-sea engineering require knowledge of mechanical and transport properties. The presence of gas hydrate effects sea-floor slope stability.

This paper describes how nuclear magnetic resonance (NMR) is used to assay ice or hydrate in cores. Moreover, it provides estimates of relative permeability to water, and furnishes unique information about the pore-scale interaction of ice or hydrate with host sediments. First, the properties of permafrost and gas hydrate are briefly reviewed, and the basic principles of NMR are laid out. Then the applications of NMR to the study of frozen core are described in detail. Finally, two field studies are used to illustrate the information available from magnetic resonance measurements.

Permafrost

Permafrost is continuously frozen soil present in arctic regions (Anderson & Morgenstern 1973). The upper limit of permafrost is typically within a few metres of the land surface, and the lower limit is controlled by the long-term mean surface temperature and the geothermal gradient (Lachenbruch *et al.* 1982). The base of permafrost is not necessarily at the 0 °C isotherm, and may in fact be substantially shallower (Collett & Bird 1988; Collett *et al.* 1993).

Not all water in permafrost is frozen. The amount of unfrozen water depends on temperature, pressure, water salinity, and the mineralogy and specific surface area of the soil (Dillon & Andersland 1966; Anderson & Tice 1972; Anderson & Morgenstern 1973). Unfrozen water has substantial effects on mechanical and transport properties, including the strength of the sediment, speed of sound, thermal conductivity and permeability to water flows. Thus, unfrozen water content is important to both civil engineers and geophysicists.

Sampling of permafrost formations requires some care since it is desirable to maintain the core below 0 °C. Coring subsurface formations normally requires the use of a drilling fluid, which will melt ice. However, if the operation is fast enough, only a thin surface layer of the whole core (typical diameter 10 cm) will be affected. Plugs can be drilled from the frozen centre of the core in a chilled laboratory.

Numerous methods can be used to quantify unfrozen water in sediment. Classical methods such as dilatometry, calorimetry and differential thermal analysis are reviewed by Anderson & Morgenstern (1973). In recent years non-destructive methods have predominated. Nuclear magnetic resonance (Tice *et al.* 1982; Smith & Tice 1988) is fast and accurate. The NMR assay is based on a large contrast in magnetic-relaxation times of water in solid and liquid phases, as explained below. Dielectric constant techniques (Smith & Tice 1988), which are based on differing electromagnetic propagation speeds through liquid and solid, have similar advantages.

Gas hydrates

Gas hydrates are clathrate compounds in which individual small molecules (which are commonly,

From: ROTHWELL, R.G. 2006. *New Techniques in Sediment Core Analysis*. Geological Society, London, Special Publications, **267**, 179–192. 0305-8719/06/$15.00

but not exclusively, in the gas phase at room temperature and pressure) occupy sites within a crystalline matrix of water molecules (Sloan 1998). There are three structural forms, distinguished by crystal structure and the sizes of the cages, in which the guest molecules reside. The most common form in nature is Structure I, which is exemplified by methane hydrate. The composition is $G_x \cdot (H_2O)_6$, where G is the guest species and x is approximately 1 for Structure I hydrate.

Gas hydrates form at elevated pressure and reduced temperature, conditions that are satisfied in both marine and terrestrial environments (Kvenvolden 1993). In the ocean, hydrate can exist below the depth at which the pressure–temperature profile crosses the phase boundary, typically around 500 m. It does not exist in the ocean proper because it is less dense than water. However, it is readily trapped in sediments and is stable down to the depth at which the geothermal gradient of the solid earth recrosses the phase line, typically several hundred metres below the sea floor. Hydrates are also stable in a band of depths below the surface in arctic regions, overlapping and below the range of permafrost stability.

The creation of gas hydrate deposits requires a source of gas. Seeps of natural gas, consisting mostly of methane, are common in many parts of the world, and so are hydrate accumulations. The total amount of hydrocarbon gas trapped in hydrates is immense, and has significant implications for sourcing of fossil fuel and for global climate change (Kvenvolden 1993).

Collection and preservation of hydrate core samples is a significant problem. Whereas permafrost only needs to be kept at subsurface temperature to maintain a core sample in its original state, hydrate-affected samples must be kept under pressure, a significantly more difficult problem (ODP Shipboard Scientific Party 2003; Schultheiss *et al.* 2006). Moreover, it is essentially impossible to reconstitute a hydrate core sample to its original state: once the core exits the temperature and pressure ranges over which hydrate is stable, evolved gas tends to redistribute both itself and the melt water, and can even disaggregate the sample.

There are a number of methods of quantifying the amount of gas hydrate in rock and sediment core samples. The most commonly used technique is indirect and destructive of the sample. Hydrate decomposition releases fresh water, thereby changing the pore-water salinity. Comparing the observed pore-water salinity to an assumed background depth profile permits computation of the original hydrate content (Dickens *et al.* 1997).

The formation of hydrate in unconsolidated sediment has a stiffening effect, so measurement of the speed of sound would appear to be a good technique for determining hydrate content. However, these estimates of hydrate concentration depend on whether the hydrate preferentially cements grains at their contacts, coats grains uniformly, partially supports the frame, floats freely in the pore space, or forms isolated lenses and nodules. As the microgeometry of hydrate disseminated in porous media is unknown, quantitative determinations of hydrate content from wave-speed measurements are uncertain. Other parameters of the interpretation models include the amounts and acoustical properties of the various minerals composing the matrix and their degree of cementation, which may or may not be known.

Because saline pore water is a good conductor of electricity and hydrate is an insulator, electrical resistivity measurements have also been used to characterize hydrate core samples. However, interpretation of these measurements depends on empirical models with poorly constrained parameters that depend on sediment properties and on the hydrate saturation itself (Spangenberg 2001). They also require knowledge of pore-water salinity, which is a problem when the formation or dissociation of hydrate creates pore-water anomalies.

Dielectric constant measurements avoid many of the problems of acoustic and low-frequency electrical measurements. The dielectric constant has some sensitivity to pore-water salinity and hydrate microgeometry, but these are secondary effects. Dielectric constant has been used to measure the presence of hydrate in several investigations (Boissonnas *et al.* 2000; Wright *et al.* 2002).

Nuclear magnetic resonance measurements

Nuclear magnetic resonance (more briefly, magnetic resonance or NMR) is well known for being able to provide information about molecular structure and motion, and images of the human body. Less well known is its ability to investigate porous media (Kleinberg 1999). NMR is now widely used in the oil and gas industry to characterize the productive potential of hydrocarbon reservoirs (Kleinberg 1996*a*; Kleinberg & Flaum 1998).

Basic principles

To make an NMR measurement in the laboratory, a sample is placed inside a magnet and a coil. Magnetic nuclei are first aligned by the

static magnetic field B_0, generated by a large electromagnet or superconducting solenoid. Then the nuclei are irradiated by the coil, which transmits pulses with a carrier frequency $f_0 = (\gamma/2\pi)B_0$, where γ is the gyromagnetic ratio of the nucleus. γ is different for each type of nucleus. Hydrogen is the most commonly probed nuclear species, and for hydrogen nuclei $\gamma/2\pi = 42.58\,\mathrm{MHz\,T^{-1}}$. The pulses reorient the magnetic moments of the nuclei.

Measurements of magnetic relaxation have proved to be particularly helpful in porous media studies. The transverse relaxation (T_2) measurement consists of a series of pulses. The first pulse rotates the nuclei 90° from the B_0 direction. This is followed by a long series of 180° pulses. When irradiated with this series of pulses, a nuclear spin system will return a series of equally spaced spin echoes, one after each 180° pulse. The echo spacing, T_E, is typically a fraction of a millisecond. The transverse magnetization decay is monitored by measuring the amplitudes of the echoes during the sequence. An entire decay curve is acquired during one echo train, which makes this measurement very efficient. The characteristic decay time of echo amplitude, T_2, is the transverse relaxation time.

The initial amplitude of the decaying proton NMR signal is proportional to the hydrogen content of the sample. The signal from hydrogen locked in solid minerals decays orders of magnitude faster than the signal from hydrogen in liquids. Thus, the signal from the solid is easily excluded from the amplitude measurement by, for example, making the echo spacing (and therefore the time before the first echo) longer than the solid signal relaxation time. Ice and both host and guest components of gas hydrates respond like solids, so they are invisible in NMR measurements designed to be insensitive to solids.

NMR of porous media

The NMR relaxation rate of fluids in porous media is controlled in part by relaxation at the pore–grain interface. Molecules in a fluid diffuse, eventually reaching a grain surface where their nuclear spins can be relaxed. In sediments and sandstones, the rate-limiting step is the relaxation process at the surface, not the transport of unrelaxed spins to the surface (Kleinberg *et al.* 1994). The decay rate due to surface processes, $1/T_{2S}$, does not depend on pore shape but only on the surface-to-volume ratio, S/V, of the pore:

$$\frac{1}{T_{2S}} = \rho_2 \left(\frac{S}{V}\right)_{\mathrm{pore}}. \qquad (1)$$

Thus, water in small pores relaxes rapidly, while water in large pores relaxes more slowly. The surface-relaxivity coefficient ρ_2 is a characteristic of magnetic interactions at the fluid–solid interface (Kleinberg *et al.* 1994; Foley *et al.* 1996). In sands and analogous materials it is dominated by paramagnetic centres at grain surfaces.

There are two other NMR relaxation mechanisms. One of them occurs in bulk liquids, and is independent of the presence of porous media. Another is associated with molecular diffusion through magnetic field gradients. These processes operate in parallel, so the observed magnetization decay of fluid in a single pore is:

$$M(t) = M_0 \exp\left[-\frac{t}{T_2}\right] \qquad (2)$$

where M_0 is the spin-echo amplitude extrapolated to the start of the measurement sequence and

$$\frac{1}{T_2} = \frac{1}{T_{2B}} + \frac{1}{T_{2S}} + \frac{1}{T_{2D}} \qquad (3)$$

T_{2B} is the bulk relaxation time. T_{2D} is a relaxation time connected with diffusion, and is discussed further below.

Rocks and sediments generally have very broad distributions of pore sizes, and therefore the magnetization decays can be expressed as a sum of exponential decays (Gallegos & Smith 1988):

$$M(t) = \sum_i m_i \exp\left[-\frac{t}{T_{2i}}\right] \qquad (4)$$

where m_i is proportional to the volume of fluid relaxing at the rate $1/T_{2i}$. The sum of the volumes is proportional to the fraction of the material occupied by liquid, the porosity ϕ_{NMR}:

$$M_0 = \sum_i m_i \approx \phi_{\mathrm{NMR}}. \qquad (5)$$

To analyse the measurements, the monotonic but non-exponential magnetization decays are fitted to equation (4), where $M(t)$ typically represents the amplitudes of thousands of spin echoes equally spaced in time, and the T_{2i} are typically 30–50 preselected time constants, equally spaced on a logarithmic scale over the range from tenths of milliseconds to seconds. The number of terms in the summation is somewhat arbitrary, since the exponentially decaying basis functions are not linearly independent. In fact, there are far less than 30 independent pieces of information in a typically noisy decay. Therefore, the set of $m_i(T_{2i})$ are found using a

regularized non-linear least-squares technique that renders the results smooth and stable in the presence of random noise (Butler *et al.* 1981). The function $m(T_2)$ is conventionally called a T_2 distribution.

Bulk relaxation depends only on the temperature and pressure of the fluid and is easily accounted for. The mechanism connected with diffusion through magnetic field gradients poses more important problems. When this process is significant compared to the first two, the relaxation-time distributions are difficult or impossible to interpret. Magnetic field gradients exist in sediments and rocks due to the magnetic susceptibility contrast between diamagnetic pore fluids and paramagnetic mineral grains, which in common sands are about 1% iron. The effect depends strongly on the applied magnetic field B_0. It is very desirable to employ NMR apparatus using low magnetic field (less than about 0.1 T) for core studies (Kleinberg & Horsfield 1990; Kleinberg 1999).

At low field, for most sandstones and sand sediments, both the bulk and magnetic field gradient relaxation processes are negligible compared to the surface relaxation process. Then equation (1) can be used to estimate pore size from NMR relaxation time. A pore-space model is required to find pore diameter from the surface to volume ratio. A convenient model is a network of interconnected cylindrical tubes; this is the model used (often implicitly) for mercury porosimetry analysis of natural earth materials. In this model, the surface-to-volume ratio of a pore is $S/V = 4/D$, where D is the pore diameter. Although this transform from relaxation time to pore size is not rigorous, it has been found to be widely useful.

The NMR-derived pore-size distribution of a typical sandstone is shown in Figure 1. The area under the curve is proportional to the liquid-filled porosity ϕ_{NMR}. The lower axis is the relaxation time plotted on a logarithmic scale. The upper axis shows the corresponding pore sizes, calculated assuming the pores are cylindrical. Thus, the NMR-determined pore diameter is related to the relaxation time T_2 by:

$$D = 4\rho_2 T_2. \tag{6}$$

The surface relaxivity of Berea sandstone, obtained by comparing mercury porosimetry to NMR data (Kleinberg 1999), is $\rho_2 = 11\,\mu m\,s^{-1}$. This value is within the usual range of relaxivities of oil reservoir sandstones, which average about $5\,\mu m\,s^{-1}$.

Water associated with clay minerals has a distinct signature in the T_2 distribution. It is commonly observed that T_2 distributions of sandstones have a foot at $T_2 < 3$ ms (Kleinberg 1996*b*), which is correlated with the quantity of clay-bound water (Straley *et al.* 1994). The distinctiveness of clay-bound water in the T_2 distribution indicates that it does not exchange with pore water on the timescale of the NMR measurement (Kleinberg 1999).

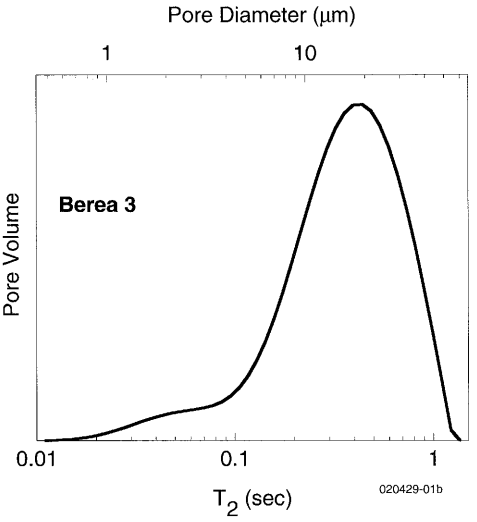

Fig. 1. NMR relaxation-time distribution for a typical sandstone. The area under the curve is proportional to the liquid-water-filled porosity ϕ_{NMR}. The corresponding pore-diameter distribution (upper axis) is computed using equation (6) with $\rho_2 = 11\,\mu m\,s^{-1}$.

Further information on the capabilities and limitations of NMR measurements of rocks and sediments are available in a review (Kleinberg 1999).

Applications of NMR to the study of frozen core

Unfrozen water

There are a number of reasons why water in soil remains unfrozen below 0 °C, including salinity and capillary pressure effects. The depression of the freezing point by capillary forces is (Adamson 1976; Morishige & Kawano 1999):

$$\Delta T = T_m \frac{4\gamma_{sl}}{Q_f \rho_s D} \tag{7}$$

where T_m is the normal melting point, γ_{sl} is the surface tension of the solid–liquid interface, Q_f is heat of fusion per gram, ρ_s is the density of

the solid and D is the diameter of the cylindrical capillary. For the water–ice transition, $T_m = 273.15\,K$, $Q_f = 334\,kJ\,kg^{-1}$ and $\rho_s = 916.2\,kg\,m^{-3}$. The surface tension of the water–ice interface is uncertain; Franks (1982) cites values ranging from 19.7 to 44 $mJ\,m^{-2}$ (excluding one value at 6.4 $mJ\,m^{-2}$), which average to $\gamma_{sl} = 28.3\,mJ\,m^{-2}$. Using these values we find $\Delta T = (0.1\,\mu m{\cdot}K)/D$.

In the permafrost experiments described below, the lowest temperature to which the core samples were exposed was −14 °C. This is just cold enough to freeze water in 0.007 μm-diameter pores, which are the smallest pores to which the NMR measurements were sensitive. As the temperature increased, ice in successively larger pores melted.

Water intimately associated with clay constitutes a distinct fraction of the water found in rocks and soils. As noted in the subsection on 'NMR of porous media' earlier, clay-bound water is correlated with NMR relaxation times in the range $T_2 < 3$ ms. Differential thermal analysis shows that some clay-associated water does not freeze until the temperature is lowered to the range $-60\,°C < T < -35\,°C$ (Anderson & Tice 1971). A fraction of water in coal is unfrozen down to −125 °C (Mraw & Naas-O'Rourke 1979). Thus, at least some of the water associated with clay and coal is not expected to be frozen in naturally occurring permafrost.

Quantitative assay of ice or hydrate

NMR spectrometers sensitive to hydrogen in solids have been used to measure structure and properties of gas hydrate in bulk (Davidson & Ripmeester 1978; Ripmeester & Ratcliffe 1988). However, in order that the electronic dead time be shorter than the relaxation times of nuclei in solids, high-frequency (high B_0, e.g. 4 T) measurements are necessary. However, as pointed out above, core studies require very low applied magnetic fields, 0.1 T or less. Thus, measurements that are most useful for probing pore-scale effects in sediments and rock cores are blind to ice and hydrate. NMR would not appear to be helpful in quantifying the frozen constituents of cores.

However, when NMR is combined with a measurement of porosity that does not distinguish between frozen and unfrozen pore water, reliable and quantitative measurements of ice or hydrate saturation are possible. The difference between total porosity and the NMR indication of liquid-water content gives the amount of frozen material present in the measurement volume.

There are a number of methods of determining total porosity. For consolidated rock, the sample is thawed and the porosity determined by the standard Archimedes method. Unconsolidated sediments present more challenges. If a permafrost sample is contained in a non-metallic sample tube, or retains cohesion, the thawed sample can be remeasured by NMR and the result corrected for the 8% shrinkage of water upon melting. Hydrates in sediment require further care, as water can be expelled from the sample when gas is liberated upon thawing.

A useful technique for both permafrost and hydrate samples is to measure the mass density of the unthawed sample using a gamma-ray densitometer (Blum 1997). The bulk density ρ_b is

$$\rho_b = (1-\phi)\rho_m + \phi S_w \rho_w + \phi(1-S_w)\rho_i \quad (8)$$

where ρ_m, ρ_w and ρ_i are the mass densities of the mineral matter, the liquid water and the frozen (ice or hydrate) phase, respectively, ϕ is the porosity, S_w is the water saturation (fraction of pore space occupied by liquid water), and $1 - S_w = S_i$ is the saturation of the frozen phase. The apparent NMR porosity is

$$\phi_{NMR} = \phi S_w \quad (9)$$

so

$$\phi = \phi_{NMR}\frac{(\rho_w - \rho_i)}{(\rho_m - \rho_i)} + \frac{(\rho_m - \rho_b)}{(\rho_m - \rho_i)} \quad (10)$$

$$S_i = 1 - \frac{\phi_{NMR}}{\phi}. \quad (11)$$

The density of methane hydrate, which is not stoichiometric, depends on its composition and is generally in the range of 900 $kg\,m^{-3}$ (Collett 1998).

Pore-scale distribution of frozen components

Nuclear magnetic resonance has the unique capability of determining the sizes of pores in which liquid water resides. When invisible to NMR, the presence of ice or gas hydrate diminishes the integrated amplitude and changes the shape of the apparent (i.e. liquid-filled) pore-size distribution. These changes depend on where the solid resides within the pore space, and on the magnetic coupling between pore water and the solid. Therefore, if the pore-size distribution of the thawed sample is determined, an NMR measurement of the same material containing

ice or hydrate will indicate whether they partially or fully occupy small pores, large pores or both.

The following discussion applies equally to ice and gas hydrate. If ice coats grain surfaces, its relaxivity to liquid water, ρ_2 (water–ice), replaces ρ_2 (water–rock) in equation (1). In principle, pore-size information will be retained, but the transformation between T_2 and pore diameter is changed. On the other hand, if the ice grows in the interior of pores, its surfaces add to the silica grain surfaces and equation (1) must be generalized to account for the simultaneous influence of two different surfaces.

The relaxivity of the ice–water surface is unknown, but the following end-member scenarios can be identified:

- Ice coats grain surfaces and ρ_2 (water–ice) $\ll$ ρ_2 (water–rock): in all but the smallest pores, the bulk relaxation process will dominate, and the relaxation-time distribution $m(T_2)$ will tend to pile up at the bulk relaxation time T_{2B}. The bulk relaxation time depends on temperature and pressure, but not salinity unless dissolved paramagnetic ions are present; for water at 0 °C and 1 atm, $T_{2B} = 1.59$ s (Simpson & Carr 1958).
- Ice coats grain surfaces and ρ_2 (water–ice) $\gg$ ρ_2 (water–rock): the relaxation-time distributions snap to short relaxation times at the first appearance of ice, then shrink as ice fills the pores.
- Ice preferentially fills the largest pore spaces and ρ_2 (water–ice) $\ll$ ρ_2 (water–rock): water relaxes at grain surfaces while being excluded from large pore bodies. The distributions gradually shrink and move smoothly to shorter relaxation times as freezing proceeds.
- Ice preferentially fills the largest pore spaces and ρ_2 (water–ice) $\gg$ ρ_2 (water–rock): water relaxes at both grain and ice surfaces, so the relaxation-time distribution is concentrated at short values of T_2.

In reality, the NMR response might result from a combination of these effects, for example if the grains are partially coated with ice.

Hydraulic permeability

The hydraulic permeability of a porous medium depends generally on the square of the cross-sectional dimension of the flow channels (Scheidegger 1960). The sensitivity of NMR measurements to the pore size makes it a good permeability indicator for sandstones. The NMR estimate of permeability has been tested on thousands of sandstones, for which there is order-of-magnitude agreement with conventional water or gas flux measurements (Straley *et al.* 1994). However, the technique has not been systematically tested in unconsolidated sediments, nor in sediments consolidated by ice or hydrate.

The empirical correlation that connects hydraulic permeability, k_0, to porosity and a one-parameter measure of relaxation time, T_{2LM}, is

$$k_0 = C\phi_{NMR}^4 T_{2LM}^2 \tag{12}$$

where T_{2LM} is the logarithmic mean value of the T_2 distribution

$$T_{2LM} = 10^{\left[(1/\phi)\sum_i m_i(T_{2i})\log_{10}(T_{2i})\right]}. \tag{13}$$

C is a coefficient that depends on mineralogy. A large number of measurements on water-saturated clean and clay-rich sandstones showed that typically $C = 4000\,\mathrm{D\,s^{-2}}$ (Straley *et al.* 1994) (1 darcy (D) $\approx 0.987 \times 10^{-12}$ m^2).

Just as the presence of ice or hydrate has an unknown effect on surface relaxivity, it will similarly influence the NMR permeability estimate in as-yet-unknown ways. If hydrate magnetically shields grain surfaces, or strongly relaxes water, at very least the coefficient of equation (12) will be affected.

Relative permeability is the permeability of the sediment to a single fluid when two or more constituents occupy the pore space. In a rock or sediment containing oil, water and/or or gas, each of these fluids will have a different relative permeability, which depends on the saturations. Here we use the term to describe the hydraulic permeability when the pore space is partially filled with ice or hydrate:

$$k_{rw} = \frac{k(S_w)}{k_0} \tag{14}$$

where k_0 is the permeability of the fully liquid-water-saturated sediment, and $k(S_w)$ is the permeability at water saturation S_w, with the remaining pore space filled with ice or hydrate at saturation $S_i = 1 - S_w$.

Relative permeability may be found when permeability measurements of both fully water-saturated sediment and the same sediment partially saturated with ice or hydrate are available. This is the case in permafrost thawing studies, where the NMR properties of a sample are followed over a range of water saturations. It is also the case at the base of permafrost or hydrate, to the extent that sediment properties are uniform over the transition zone. Water

saturation is found from

$$S_w = \frac{\phi_{NMR}(S_w)}{\phi_{NMR}(S_w = 1)} \quad (15)$$

where $\phi_{NMR}(S_w)$ and $\phi_{NMR}(S_w = 1)$ are apparent NMR porosities in the partially and fully water-saturated sediment, respectively. Using this and equations (12) and (14), the NMR estimated relative permeability is:

$$k_{rw} = \frac{k(S_w)}{k_0} = S_w^4 \left(\frac{T_{2LM}(S_w)}{T_{2LM}(1.0)} \right)^2. \quad (16)$$

The mineralogy dependent coefficient C does not appear in this ratio.

As noted above, this approach has some important limitations: the permeability estimate is based on an empirical correlation, not a flow measurement, and it assumes that the correlation is as valid for ice-affected sediment as it is for water-filled rock. A subsidiary assumption is that NMR relaxation of liquid water at an ice or hydrate surface is no stronger than at a mineral grain surface. It also assumes that differences of the microgeometrical distribution of water in unfrozen and partially frozen rock do not invalidate the correlation.

Core measurements using an NMR borehole logging tool

Apparatus

Most modern NMR laboratory instruments operate at high magnetic field, B_0, and correspondingly high frequency, f_0. However, the magnetic susceptibility of ordinary sands and sandstones makes this a poor strategy when investigating fluid in the pore space of rocks, as explained in the subsection on 'NMR of porous media'. Therefore specialized low-field NMR equipment is used for core studies, for example the Resonance Instruments MARAN, and the NUMAR CoreSpec instruments. These instruments, which use compact permanent magnets, are smaller and simpler to deploy to field locations than large conventional laboratory machines, some of which use superconducting magnets.

The Schlumberger Combinable Magnetic Resonance Tool (CMR) can also be used to measure core samples, and it is particularly useful for fieldwork. The CMR is an oilfield wireline logging tool rated to survive and operate in arctic, tropical, desert and marine environments. The CMR is basically cylindrical and has the unusual capability of making measurements on compact external samples (Kleinberg *et al.* 1992). Permanent magnets project a static magnetic field into an external volume. This field is relatively homogeneous over a volume approximately 15 cm long and 4 cm^2 in cross-sectional area, centred 2.5 cm from the face of the instrument. The static field strength in this volume is $B_0 = 52$ mT. An antenna transmits pulses of radiofrequency (RF) with a carrier frequency of $f_0 = 2.2$ MHz to perform transverse relaxation measurements; the same antenna receives the spin echo signals, used to monitor the magnetization decay of water protons. The effective dead time is 200 μs. The apparatus is sensitive only to the region in which the static field is relatively homogeneous. NMR cannot make measurements through metal core barrels, but is insensitive to the protons in plexiglas core barrels.

Sea-floor measurements of gas-hydrate-saturated core samples

Location and procedures. Experiments conducted at the sea floor provide opportunities to observe creation of gas hydrates under conditions that in some ways mimic natural processes (Brewer *et al.* 1997). For this reason, a remotely operated sub-sea vehicle (ROV) was equipped with the CMR and carried out a series of controlled experiments at the sea floor offshore of central California. Measurements were made at various points in the Monterey Canyon between depths of 1000 (36°47′N 122°05′W) and 3000 m (36°35′N 122°30′W) (Kleinberg *et al.* 2003*a*,*b*).

Sea-floor conditions fall easily within the specifications of the CMR, which was designed to operate at temperatures between −25 and +175 °C, pressures up to 140 MPa and water salinities up to the saturation limit of NaCl. The weight of the CMR, 133 kg, was not a serious problem for ROV deployment. However, at 4.3 m, the tool was much too long to be mounted on the vehicle. Therefore, the CMRC electronics cartridge was mounted horizontally at the bottom of the ROV. The CMRS sonde (sensor) section was mounted vertically at the front of the ROV, where its magnet and antenna were easily accessed by a manipulator arm and video cameras. A special L-coupling mated the CMRC and CMRS.

Rocks and sediments were transported and treated in 76 mm outside diameter Plexiglas tubes. Valves were provided which allowed the introduction of methane at the bottom and venting at the top. The sample tubes used for sediments were 600 mm long and had an inside diameter of 70 mm, which included 99.3% of

the resonated volume of the NMR instrument. The sample tubes used for rocks were 300 mm long and had an inside diameter of 54 mm, which included 92.5% of the resonated volume. These tubes were individually machined to minimize dead volume: the resonated volume not within the sample was entirely within the walls of the tubes, which contributed no signal. There was no evidence for signal from bulk sea water inside or outside the sample tubes.

Hydrate was grown in porous media by various methods that were hypothesized to approximate natural mechanisms. In some experiments, gaseous methane was bubbled through sea-water-saturated rocks or sediments while within the gas hydrate stability zone of the ocean. In other experiments, methane was dissolved in sea water and allowed to slowly transform to hydrate over a period of weeks.

Hydrate assay and growth habit. In the sandstones the presence of hydrate decreased the apparent NMR porosity, as expected. In one group of experiments samples were allowed to equilibrate at the sea floor at a depth of 1000 m for 1 month. The temperature was approximately 4 °C and the pressure was approximately 10 MPa. At this pressure the methane hydrate decomposition temperature is 12 °C in sea water (Henry *et al.* 1999). Thus, the core samples were well within gas hydrate stability conditions, and no free gas was expected to be present; however, there was no independent check for the presence of gas. Results for Berea sandstone are shown in Figure 2. Accuracy of the NMR measurement was established by comparing the sea-floor measurement of sandstone porosity when fully saturated with sea water (top bar) with later laboratory measurement (bottom bar).

In the presence of hydrate, the NMR signal (light shaded part of middle bar) was reduced by an amount corresponding to 0.012 of the rock volume. This agreed well with the hydrate volume estimated from the quantity of gas evolved from the sample as it was transported above the hydrate stability zone (dark shaded part of middle bar). Estimates of hydrate volume from the quantity of collected gas should be treated cautiously. Although degassing was carried out well above the hydrate stability boundary, the thermal lag of the rock and remaining gas bubbles in the pores may lead to a systematic underestimate of hydrate volume.

For a hydrate-bearing sand pack, the NMR results strongly suggest that no hydrate was formed in two 60 cm^3 volumes of investigation; visual examination revealed hydrate was localized in nodules and lenses outside these volumes.

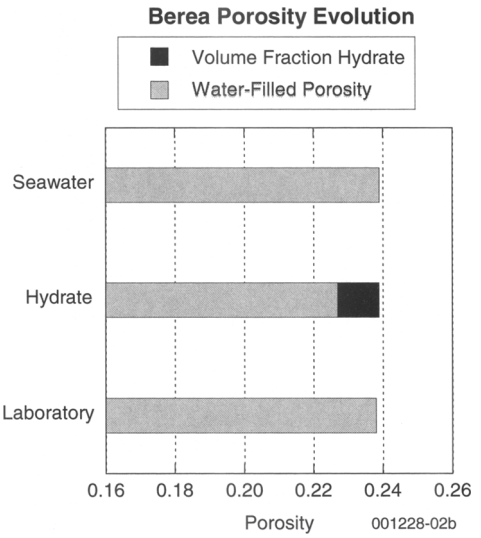

Fig. 2. NMR liquid-water-filled porosity measurements (light bars) of Berea sandstone at the sea floor fully saturated with sea water (top), at the sea floor partially saturated with hydrate (middle) and in the laboratory fully saturated with salt water (bottom). As hydrate is invisible to the CMR, the apparent porosity is reduced in its presence. The reduction agrees with a hydrate assay based on gas-evolution measurements made when the sample was transported above the hydrate stability zone (dark bar).

By contrast, in the rock samples, the loss of liquid water in the volume of investigation was proportional to the hydrate content of the rocks as a whole. Thus, the measurements were consistent with generally uniform dissemination of hydrate throughout the sandstone samples.

The observation of large nodules and lenses in the sand pack, contrasted to the uniform dissemination of hydrate in the consolidated rock, is central to understanding natural gas hydrate deposits. Bulk hydrate can only form when sand and silt grains are excluded from a growing mass of hydrate. In rock already consolidated, or cemented by the first appearance of hydrate, bulk hydrate cannot form. The presence of hydrate lenses and nodules in drill core (see, for example, Uchida *et al.* 1999) can only be explained if hydrate does not promptly cement unconsolidated sediments.

Drilling rig measurements of permafrost

Location and procedures. NMR measurements of permafrost core were made on the Anadarko Hot Ice 1 drilling rig, located approximately 35 km south of the Arctic coast of Alaska

(70°07′N 150°13′W) (Kleinberg & Griffin 2005). Continuous 7.6 cm-diameter core was taken from surface to 428 m during March and April 2003. The lithologies in the drilled interval are unconsolidated fine sands, clays or muds, ice lenses typically thinner than 1 cm, and coals.

A mobile arctic core laboratory was installed on the drilling rig, and special techniques were used to preserve the integrity of the permafrost core. After drilling each 3 m interval, a wireline-retrieved core barrel was recovered from the well. The core was extracted, cut into 1 m lengths, and immediately delivered to a core analysis trailer adjacent to the rig floor for petrographic description and NMR measurement using the CMR. The wellbore was maintained at approximately −3 °C, the rig floor and cutting shack were typically −14 °C, and the core analysis trailer was maintained near −3 °C. Generally speaking, approximately 60 min elapsed from the time the core was recovered at the wellhead to the start of NMR measurements, which took approximately 5 min each.

Typically, each 1 m-long core was measured at one location; hence, the coverage was 15 cm per metre of core length. Some attempt was made to minimize selection bias. However, grossly washed-out sections and conglomerates were both undersampled as measurements of those intervals would be meaningless in any event. Visible ice lenses, which comprised a very small fraction of the recovered core, were generally excluded from the measured volumes as the goal of the investigation was to understand how permafrost interacts with the pore space of the sediment.

The CMR is sensitive to electromagnetic interference at 2.2 MHz, and to broadband noise sources in general. To minimize measurement noise, a 38 cm-diameter, 85 cm-long open-ended wood-frame copper screen was used to shield the tool antenna and core sample. It was found that when core protruded from the end of the shield it conducted significant interference to the antenna.

Ice assay and growth habit. The apparent permafrost NMR porosity (liquid-water-filled pore space as a fraction of total sediment volume) was generally less than 0.1, considerably lower than would be expected for shallow unfrozen liquid-water-saturated sediments. In contrast, coals were characterized by unfrozen water contents of about 0.20–0.25 of total volume, in qualitative agreement with previous work. At the base of permafrost, which occurred within a reasonably massive sand body, NMR-determined porosity increased rapidly over an interval

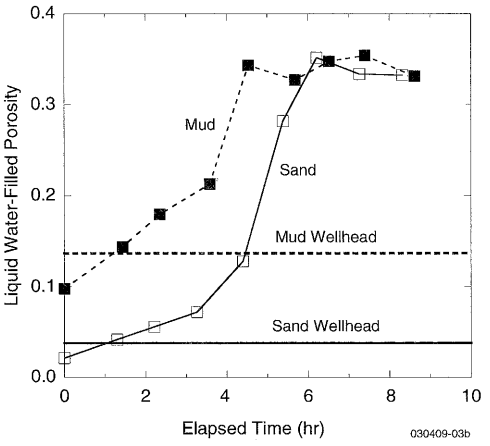

Fig. 3. Thawing of mud and sand cores monitored by NMR porosity measurements. The cores were precooled to −14 °C, then warmed in an 18 °C room. The horizontal lines indicate the porosity measurements immediately after retrieval of the core from the borehole at approximately −3 °C. When fully thawed, 92% of the pore space is occupied by liquid water and the remainder is occupied by air.

of 4 m. A systematic increase in NMR-determined unfrozen water content was an earlier indication of the base of permafrost than was petrographic examination.

Two typical 30 cm lengths of core, a sand (from depth 211 m) and a mud (from depth 202 m), were removed from storage at −14 °C and allowed to thaw in an 18 °C room. NMR measurements were made on the cores approximately once per h for 9 h. The unfrozen water porosities are plotted as a function of time in Figure 3. The sand started with significantly less unfrozen water than the mud. The mud completely thawed in 4.5 h, and the sand in 6 h. The data reflect conditions in a volume centred 2.5 cm from the surface of the 7.6 cm-diameter cores, as described in subsection on 'Apparatus'.

In both cases significantly less unfrozen water volume was found at −14 °C than when the core was first removed from the well at a temperature of approximately −3 °C. The wellhead values of apparent NMR porosity are denoted by horizontal lines in Figure 3. As the density of ice is 920 kg m^{-3}, the pore space was not completely water-saturated upon thawing so, in the absence of sediment shrinkage, 8% of the pore space was occupied by air after all the ice had melted.

Relaxation-time distributions are shown in Figure 4 for the mud and in Figure 5 for the sand. The pore-space model used to convert relaxation time, lower axes, to pore diameter,

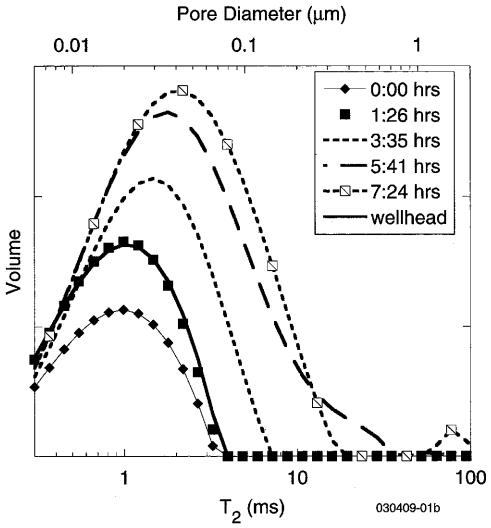

Fig. 4. Relaxation-time distributions of mud during thawing from −14 to 18 °C. Frozen samples are characterized by low NMR amplitudes and short relaxation times. After 1.5 h of warming (solid squares) the core returned to the state in which it was removed from the wellbore (heavy solid line). During the melting process the amount of NMR-visible (liquid) water increased, and successively larger pore spaces thawed. By 7.5 h (outermost line) the permafrost had completely melted, revealing the relaxation-time distribution of the water-saturated sediment. The corresponding pore-diameter distribution (upper axis) is computed using equation (6) with $\rho_2 = 5\,\mu m\,s^{-1}$.

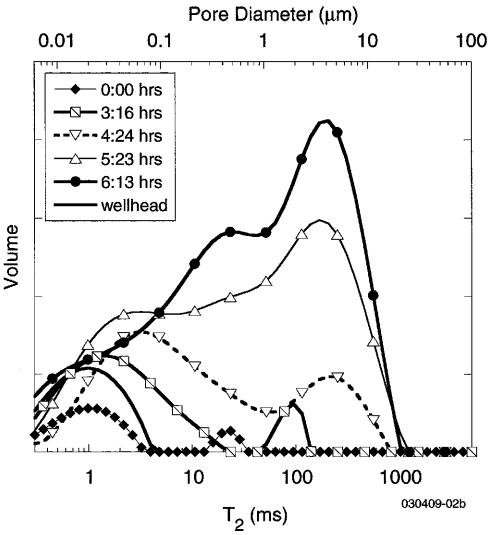

Fig. 5. Relaxation-time distributions of sand during thawing from −14 to 18 °C. Frozen samples are characterized by low NMR amplitudes and short relaxation times. During the melting process the amount of NMR-visible (liquid) water increased, and successively larger pore spaces thawed. By 6.25 h (topmost line) the permafrost had completely melted, revealing the relaxation-time distribution of the water-saturated sediment. The corresponding pore-diameter distribution (upper axis) is computed using equation (6) with $\rho_2 = 5\,\mu m\,s^{-1}$.

upper axes, is the network of interconnected cylindrical tubes described in the subsection on 'NMR of porous media'. The assumed relaxivity parameter is $\rho_2 = 5\,\mu m\,s^{-1}$.

For both sand and mud, the frozen cores are characterized by low-amplitude distributions at $T_2 < 3$ ms. Some of this water could be in small pores, in which the freezing point is depressed due to capillary forces, see equation (7). Much of the unfrozen water is very probably clay-bound water, described in the subsections on 'NMR of porous media' and 'Unfrozen water', which does not freeze at naturally occurring temperatures. As the cores thawed, amplitude increased, especially at the longest relaxation times. In both Figure 4 and Figure 5 the topmost curves represent the thawed 92% liquid-water-saturated pore-size distributions.

These data are not due to a thermal gradient within the NMR volume of investigation, 4 cm^2 in cross-section centred 2.5 cm from the core surface. Temperature uniformity can be tested by calculating the Biot number, $Bi = hL/k$, the dimensionless ratio of the surface heat transfer coefficient, h, the thermal conductivity of the solid, k, and the volume to surface area ratio, L (Ozisik 1980). In the present case $h = 5.4\,W\,m^{-2}\,K^{-1}$, determined from the rate of thawing. For a cylinder the volume to surface area ratio is one-quarter of the diameter so $L = 0.0188$ m. The thermal conductivity, computed using a simple mixing rule (Hearst *et al.* 2000), is $k = 4.64\,W\,m^{-1}\,K^{-1}$ for the unthawed core and $k = 3.20\,W\,m^{-1}\,K^{-1}$ for the thawed core. For both unthawed and thawed core $Bi < 0.1$. Thus, the temperature inside the cores is uniform during thawing (Ozisik 1980).

The data shown in Figures 4 and 5 allow us to narrow the range of possible growth habits of ice in sediments, as described in the subsection on 'Pore-scale distribution of frozen components'. In doing so, we assume that freezing and thawing of water in sediment is reversible, an assumption these experiments have not tested. The data are not consistent with scenario (1). If ice coated grain surfaces and ρ_2 (water–ice) $\ll \rho_2$ (water–rock), the low-temperature relaxation-time distribution would be concentrated around $T_2 =$ 1.59 s, which it is not. Since the relaxation-time

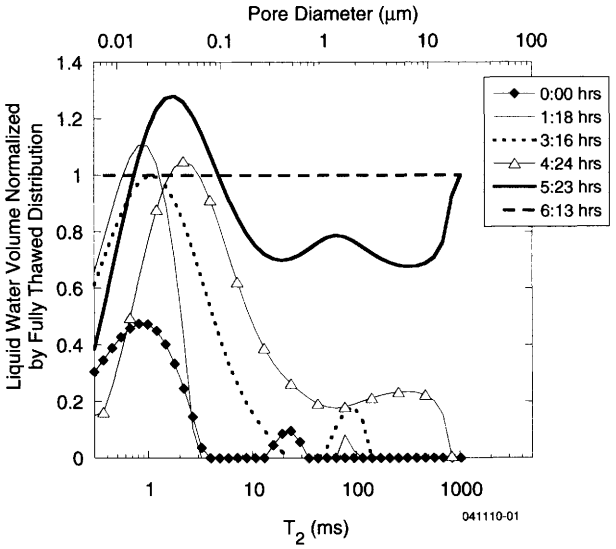

Fig. 6. Data from Figure 5 (except with data for 1 h 18 min of thawing instead of wellhead data). Each T_2 distribution has been normalized by the T_2 distribution found after 6 h 13 min of thawing.

distributions do not suddenly move to longer relaxation times at the end of the thawing process, scenarios (2) and (4) are also excluded. Thus, we conclude that liquid water is in contact with the grain surfaces, consistent with common observation (Anderson 1967; Churaev *et al.* 1993). We also conclude that the water–ice interface does not strongly relax the nuclear spins of hydrogen in liquid water.

The pore-size control of the melting of ice is illustrated by Figure 6, in which the T_2 distributions of Figure 5 are normalized by the distribution of the fully thawed sample. A temperature measurement in the interior of the core was not available, but we surmise that the curves of Figure 6 constitute an indirect thermometer. At first, ice melted in successively larger pore spaces as the temperature increased. After about 4 h of thawing, ice in pores smaller than 0.3 μm had melted, indicating that the internal temperature was within about 0.3 °C of the bulk melting temperature, according to equation (7). In larger pores the effect of pore size on melting point is negligible, and these pores thaw uniformly.

Relative permeability. Fortuitously, the base of permafrost, at a depth of 384.0 m, lay within a reasonably massive and homogeneous sand body, which constituted a natural laboratory for exploring the development of frozen sediment. The transition from fully liquid-water-saturated sediment to permafrost occurs over a depth interval of 4 m. These data, together with those from the thawed samples, were used to determine the saturation dependence of the relative permeability using equation (16).

Relative permeability estimates for the thawed samples, and for the sands at the base of permafrost are shown in Figure 7. All data follow a common trend as a function of liquid-water saturation. This is surprising as k_0 differs widely among these three datasets. The permeability of the thawed sand was 53 mD, and that of the thawed mud was 0.21 mD. The permeability of

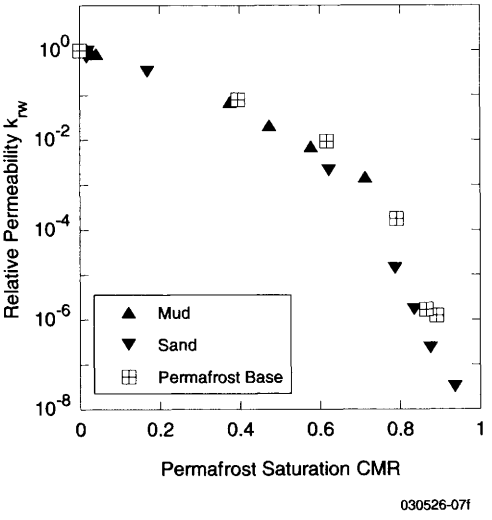

Fig. 7. Relative permeability to water computed using equation (16) for thawing mud, thawing sand and cores from the base of permafrost.

the sediment just below the base of permafrost was 14 mD. These estimates were found using equation (12) with $C = 4000\,\mathrm{D\,s^{-2}}$.

Conclusions

Nuclear magnetic resonance methods used for evaluation of oil and gas reservoirs are also useful in understanding pore-scale properties of permafrost and hydrate-bearing formations. The quantitative assay of unfrozen water content is model independent and does not depend on any adjustable parameters. However, an independent measurement of porosity is required. In the case of permafrost, this can be an NMR measurement of water content after the core has thawed. When dealing with hydrate in unconsolidated sediments, a measurement of bulk density before hydrate decomposition is desirable.

The pore-scale distribution of unfrozen water can also be obtained using NMR measurements. At the lowest temperatures attained in this study, unfrozen water appears to be associated with clay. The results of the permafrost study suggest that the silt and clay sediments investigated remain liquid-water-wet in the presence of ice, and that the water–ice interface is not effective in relaxing nuclear spins. In agreement with capillary pressure theory, ice melts first in small pores, and melts in large pores only near the end of the thawing process.

Although the permeabilities of the various sediments, as estimated by NMR, vary widely, their relative permeabilities to water as a function of ice saturation are remarkably uniform. However, the use of NMR to estimate permeability of frozen soil or rock is unproven. It would be very desirable to make fluid flux permeability measurements of samples that are also characterized by NMR.

D.D. Griffin participated in all phases of the experiments described here. P.G. Brewer and R.F. Sigal motivated the work and made available opportunities for fieldwork.

References

ADAMSON, A.W. 1976. *Physical Chemistry of Surfaces*. Wiley, New York, chap. VII-2.

ANDERSON, D.M. 1967. Ice nucleation and the substrate–ice interface. *Nature*, **216**, 563–566.

ANDERSON, D.M. & MORGENSTERN, N.R. 1973. Physics, chemistry, and mechanics of frozen ground: A review. *In*: *Second International Conference on Permafrost*. National Academy of Sciences, Washington, DC, 257–288.

ANDERSON, D.M. & TICE, A.R. 1971. Low-temperature phases of interfacial water in clay-water systems. *Proceedings of the Soil Science Society of America*, **35**, 47–54.

ANDERSON, D.M. & TICE, A.R. 1972. Predicting unfrozen water contents in frozen soils from surface area measurements. *Highway Research Record*, **393**, 12–18.

ANDERSON, D.M., PUSCH, R. & PENNER, E. 1978. Physical and thermal properties of frozen ground. *In*: ANDERSLAND, O.B. & ANDERSON, D.M. (eds) *Geotechnical Engineering for Cold Regions*. McGraw-Hill, New York, section 2.4.

BLUM, P. 1997. *Physical Properties Handbook: A Guide to the Shipboard Measurement of Physical Properties of Deep-sea Cores*. Ocean Drilling Program Technical Note, **26**, chap 3. Online at: http://www-odp.tamu.edu/publications/tnotes/tn26/ (accessed 22 October 2004).

BOISSONNAS, R., GOLDBERG, D. & SAITO, S. 2000. Electromagnetic modeling and *in situ* measurement of gas hydrate in natural marine environments. *In*: HOLDER, G.D. & BISHNOI, P.R. (eds) *Gas Hydrates: Challenges for the Future. Annals of the New York Academy of Sciences*, **912**, 159–166.

BREWER, P.G., ORR, F.M., JR, FRIEDERICH, G., KVENVOLDEN, K.A., ORANGE, D.L., MCFARLANE, J. & KIRKWOOD, W. 1997. Deep ocean field test of methane hydrate formation from a remotely operated vehicle. *Geology*, **25**, 407–410.

BUTLER, J.P., REEDS, J.A. & DAWSON, S.V. 1981. Estimating solutions of first kind integral equations with nonnegative constraints and optimal smoothing. *SIAM Journal of Numerical Analysis*, **18**, 381–397.

CHURAEV, N.V., BARDASOV, S.A. & SOBOLEV, V.D. 1993. On the non-freezing water interlayers between ice and a silica surface. *Colloids and Surfaces*, **A79**, 11–24.

COLLETT, T.S. 1998. *Well Log Characterization of Sediment Porosities in Gas Hydrate-bearing Reservoirs*. Society of Petroleum Engineers Paper, **49298**.

COLLETT, T.S. & BIRD, K.J. 1988. Freezing-point depression at the base of ice-bearing permafrost on the North Slope of Alaska. *In*: *Fifth International Conference on Permafrost, Volume 1*. Tapir, Trondheim, 50–55.

COLLETT, T.S., BIRD, K.J. & MAGOON, L.B. 1993. Subsurface temperatures and geothermal gradients on the North Slope of Alaska. *Cold Regions Science & Technology*, **21**, 275–293.

DAVIDSON, D.W. & RIPMEESTER, J.A. 1978. Clathrate ices – recent results. *Journal of Glaciology*, **21**, 33–49.

DICKENS, G.R., PAULL, C.K. & WALLACE, P. 1997. Direct measurement of *in situ* methane quantities in a large gas hydrate reservoir. *Nature*, **385**, 426–428.

DILLON, H.B. & ANDERSLAND, O.B. 1966. Predicting unfrozen water contents in frozen soils. *Canadian Geotechnical Journal*, **3**, 53–60.

FOLEY, I., FAROOQUI, S.A. & KLEINBERG, R.L. 1996. Effect of paramagnetic ions on relaxation of fluids at solid surfaces. *Journal of Magnetic Resonance*, **A123**, 95–104.

FRANKS, F. 1982. The properties of aqueous solutions at subzero temperatures. *In*: FRANKS, F. (ed.)

Water, A Comprehensive Treatise, Volume 7: Water and Aqueous Solutions at Subzero Temperatures. Plenum, New York.

GALLEGOS, D.P. & SMITH, D.M. 1988. A NMR technique for the analysis of pore structure: Determination of continuous pore size distributions. *Journal of Colloid and Interface Science*, **122**, 143–153.

HEARST, J.R., NELSON, P.H. & PAILLET, F.L. 2000. *Well Logging for Physical Properties*. Wiley, Chichester.

HENRY, P., THOMAS, M. & CLENNELL, M.B. 1999. Formation of natural gas hydrates in marine sediments 2. Thermodynamic calculations of stability conditions in porous sediments. *Journal of Geophysical Research*, **104**, (B10), 23 005–23 022.

KLEINBERG, R.L. 1996*a*. Well logging. *In*: *Encyclopedia of Nuclear Magnetic Resonance, Volume 8*. Wiley, Chichester, 4960–4969.

KLEINBERG, R.L. 1996*b*. Utility of NMR T_2 distributions, connection with capillary pressure, clay effect, and determination of the surface relaxivity parameter ρ_2. *Magnetic Resonance Imaging*, **14**, 761–767.

KLEINBERG, R.L. 1999. Nuclear magnetic resonance. *In*: WONG, P.-Z. (ed.) *Experimental Methods in the Physical Sciences, Volume 35, Methods in the Physics of Porous Media*. Academic Press, San Diego, chap. 9.

KLEINBERG, R.L. & FLAUM, C. 1998. Review: NMR detection and characterization of hydrocarbons in subsurface earth formations. *In*: BLUMLER, P., BLUMICH, B., BOTTO, R. & FUKUSHIMA, E. (eds) *Spatially Resolved Magnetic Resonance*. Wiley-VCH, Weinheim, chap. 54.

KLEINBERG, R.L. & GRIFFIN, D.D. 2005. NMR measurements of permafrost: Unfrozen water assay, pore scale distribution of ice, and hydraulic permeability of sediments. *Cold Regions Science and Technology*, **42**, 63–77.

KLEINBERG, R.L. & HORSFIELD, M.A. 1990. Transverse relaxation processes in porous sedimentary rock. *Journal of Magnetic Resonance*, **88**, 9–19.

KLEINBERG, R.L., FLAUM, C., GRIFFIN, D.D., BREWER, P.G., MALBY, G.E., PELTZER, E.T. & YESINOWSKI, J.P. 2003*a*. Deep sea NMR: Methane hydrate growth habit in porous media and its relationship to hydraulic permeability, deposit accumulation, and submarine slope stability, *Journal of Geophysical Research*, **108**, (B10), 2508, doi:10.1029/2003JB002389.

KLEINBERG, R.L., FLAUM, C. *ET AL.* 2003*b*. Seafloor nuclear magnetic resonance assay of methane hydrate in sediment and rock. *Journal of Geophysical Research*, **108**, (B3), 2137, doi:10.1029/2001JB000919.

KLEINBERG, R.L., KENYON, W.E. & MITRA, P.P. 1994. Mechanism of NMR relaxation of fluids in rock. *Journal of Magnetic Resonance*, **A108**, 206–214.

KLEINBERG, R.L., SEZGINER, A., GRIFFIN, D.D. & FUKUHARA, M. 1992. Novel NMR apparatus for investigating an external sample. *Journal of Magnetic Resonance*, **97**, 466–485.

KVENVOLDEN, K.A. 1993. Gas hydrates – Geological perspective and global change. *Reviews of Geophysics*, **31**, 173–187.

LACHENBRUCH, A.H., SASS, J.H. *ET AL.* 1982. Permafrost, heat flow, and the geothermal regime at Prudhoe Bay, Alaska. *Journal of Geophysical Research*, **87**, (B11), 9301–9316.

MORISHIGE, K. & KAWANO, K. 1999. Freezing and melting of water in a single cylindrical pore: The pore size dependence of freezing and melting behavior. *Journal of Chemical Physics*, **110**, 4867–4872.

MRAW, S.C. & NAAS-O'ROURKE, D.F. 1979. Water in coal pores: Low temperature heat capacity behavior of the moisture in Wyodak coal. *Science*, **205**, 901–902.

ODP SHIPBOARD SCIENTIFIC PARTY. 2003. Site 1249. *In*: TRÉHU, A.M., BOHRMANN, G. *ET AL.* (eds) *Proceedings of the Ocean Drilling Program, Initial Reports*, **204**, Ocean Drilling Program, College Station, TX, 21–28. http://www-odp.tamu.edu/publications/204_IR/VOLUME/CHAPTERS/IR204_08.PDF (accessed 22 October 2004).

OZISIK, M.N. 1980. *Heat Conduction*. Wiley, New York.

RIPMEESTER, J.A. & RATCLIFFE, C.I. 1988. Low temperature cross polarization/magic angle spinning ^{13}C NMR of solid methane hydrates: Structure, cage occupancy, and hydration number. *Journal of Physical Chemistry*, **92**, 337–339.

SCHEIDEGGER, A.E. 1960. *The Physics of Flow Through Porous Media*. Macmillan, New York.

SCHULTHEISS, P.J., FRANCIS, T.J.G. *ET AL.* 2006. Pressure coring, logging and subsampling with the HYACINTH system. *In*: ROTHWELL, R.G. (ed.) *New Techniques in Sediment Core Analysis*. Geological Society, London, Special Publications, **267**, 151–163.

SIMPSON, J.H. & CARR, H.Y. 1958. Diffusion and nuclear spin relaxation in water. *Physical Revew*, **111**, 1201–1202.

SLOAN, E.D. JR. 1998. *Clathrate Hydrates of Natural Gases*, 2nd edn. Marcel Dekker, New York.

SMITH, M.W. & TICE, A.R. 1988. *Measurement of the Unfrozen Water Content of Soils: Comparison of NMR and TDR Methods*. US Army Corps of Engineers Cold Regions Research & Engineering Laboratory Report, **88-18**.

SPANGENBERG, E. 2001. Modeling of the influence of gas hydrate content on the electrical properties of porous sediments. *Journal of Geophysical Research*, **106**, (B4), 6535–6548.

STRALEY, C., ROSSINI, D., VINEGAR, H., TUTUNJIAN, P. & MORRISS, C. 1994. *Core Analysis by Low Field NMR*. Society of Core Analysts Paper, **SCA-9404**.

TICE, A.R., OLIPHANT, J.L., NAKANO, Y. & JENKINS, T.F. 1982. *Relationship Between the Ice and Unfrozen Water Phases in Frozen Soil as Determined by Pulsed Nuclear Magnetic Resonance and Physical Desorption Data*. US Army Corps of Engineers Cold Regions Research & Engineering Laboratory Report, **82-15**.

UCHIDA, T., DALLIMORE, S.R., MIKAMI, J. & NIXON, F.M. 1999. Occurrences and X-ray computerized tomography (CT) observations of natural gas hydrate, JAPEX/JNOC/GSC Mallik 2L-38 gas

hydrate research well. *In*: DALLIMORE, S.R., UCHIDA, T. & COLLETT, T.S. (eds) *Scientific Results from JAPEX/JNOC/GSC Mallik 2L-38 Gas Hydrate Research Well, Mackenzie Delta, Northwest Territories, Canada*. Geological Survey of Canada, Ottawa, Bulletin, **544**.

WRIGHT, J.F., NIXON, F.M., DALLIMORE, S.R. & MATSUBAYASHI, O. 2002. A method for direct measurement of gas hydrate amounts based on the bulk dielectric properties of laboratory test media. *In*: *Proceedings of the Fourth International Conference on Gas Hydrates, Yokohama, Volume 2*, 745–749.